# Supporting information

# $CO_2$ Activation dominating the Dry Reforming of Methane catalyzed by Rh (111) based on Multiscale Modelling

Estefanía Díaz López[1] and Aleix Comas-Vives[1,2]*

[1]*Department of Chemistry, Universitat Autònoma de Barcelona, 08193 Cerdanyola del Vallès, Catalonia, Spain*

[2]*Institute of Materials Chemistry, TU Wien, 1060 Vienna, Austria.*

e-mail: aleix.comas@tuwien.ac.at, aleix.comas@uab.cat

**Supporting Figure 1: DFT calculations**

The Rh (111) surface was constructed from the bulk FCC configuration with a lattice parameter equal to 3.77 Å, in good agreement with the experimental value of 3.80 Å.[1]

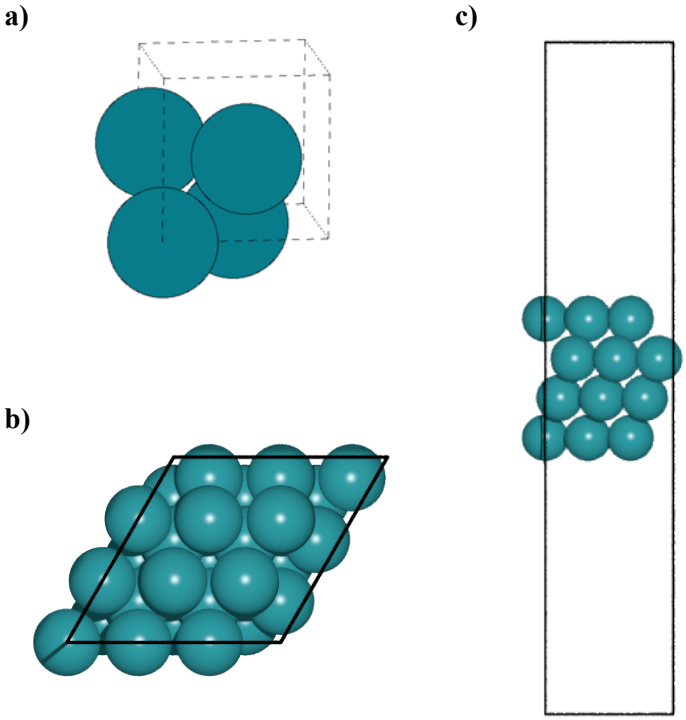


**Figure 1. a)** Bulk for Rh FCC cell, **b)** Top and **c)** side view of the 4-layered Rh (111) surface model used in this work, corresponding to a 3×3 supercell with 9 Rh atoms per layer.

**Supporting note 1. ZPE correction**

In the expressions used in this work to calculate the rate constants from standard statistical mechanical expressions[2] as we mentioned in the main text, we include the correction to the energy at the zero-point, commonly known as zero-point energy (ZPE) correction. Thus, all the energies used in the *k*MC simulations are potential energies, including the ZPE correction and relative to the reference set of species, $CH_4$, CO, $H_2$, and Rh (111). Therefore, the reference point to calculate the vibrational quasi-partition function is the first vibrational energy level ($v = 0$):

$$q_v = \prod_K \frac{1}{1 - e^{-(h\nu_K / K_B \cdot T)}}$$

As well as to affect the expression to calculate the pre-exponential factor. In this way, we obtained the rate constants including the ZPE correction.

**Supporting note 2. Stiffness scaling**

We used the stiffness scaling approach as implemented in Zacros, which employs dynamic detection of time-scale separation and a dynamic scaling of the kinetic constants to accelerate the *k*MC simulation to properly sample all the events. Zacros automatically detects the processes whose rate constants can be scalable and then it defines a "stiffness coefficient" for each event as the scaling factor of the kinetic constant of the forward and (if applicable) reverse event, which ranges from 0 to 1. Accordingly, by multiplying the pre-exponential term by a stiffness coefficient automatically determined by the program, we scaled down the rate constant of the fastest processes.[3]

**Supporting Figure 2:** *k*MC simulations at the different temperatures discussed in the main text. All *k*MC simulations shown in the supporting information do not include the disproportionation of two neighboring OH* species (OH* + OH* → $H_2O^*$ + O*) as it is not occurring, as noted in the main text, and does not affect the main conclusions.

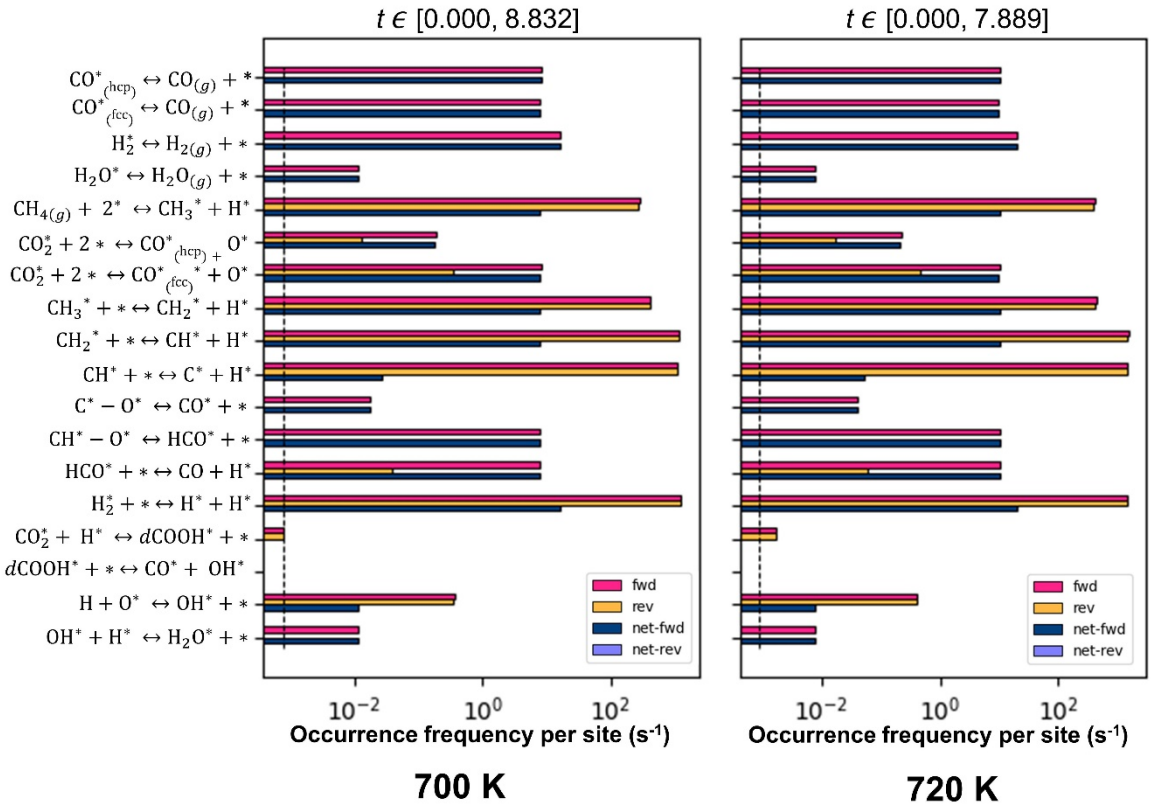

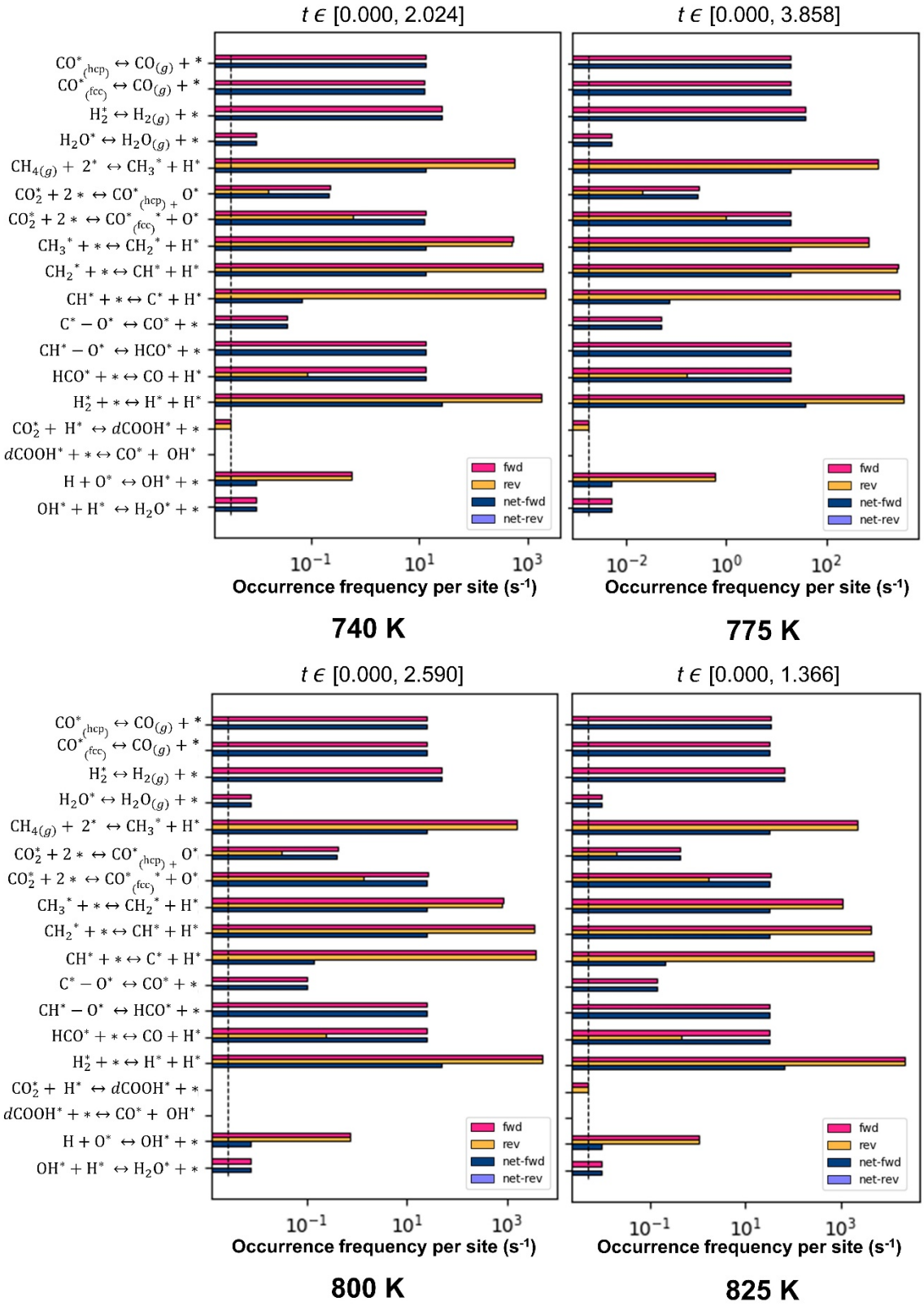


**Figure 2.** Event frequency of the dry reforming of methane reaction under four different working temperatures (a) T = 700 K; (b) T = 720 K; (c) T = 740 K; (d) T = 775 K and at steady-state.

**Supporting Figure 3**: The convergence test for the *k*MC simulations run at 700 K and 825 K. We considered that once the TOF becomes practically constant, with small fluctuations (< 0.0035), the simulation is converged, and the system reaches the steady-state.

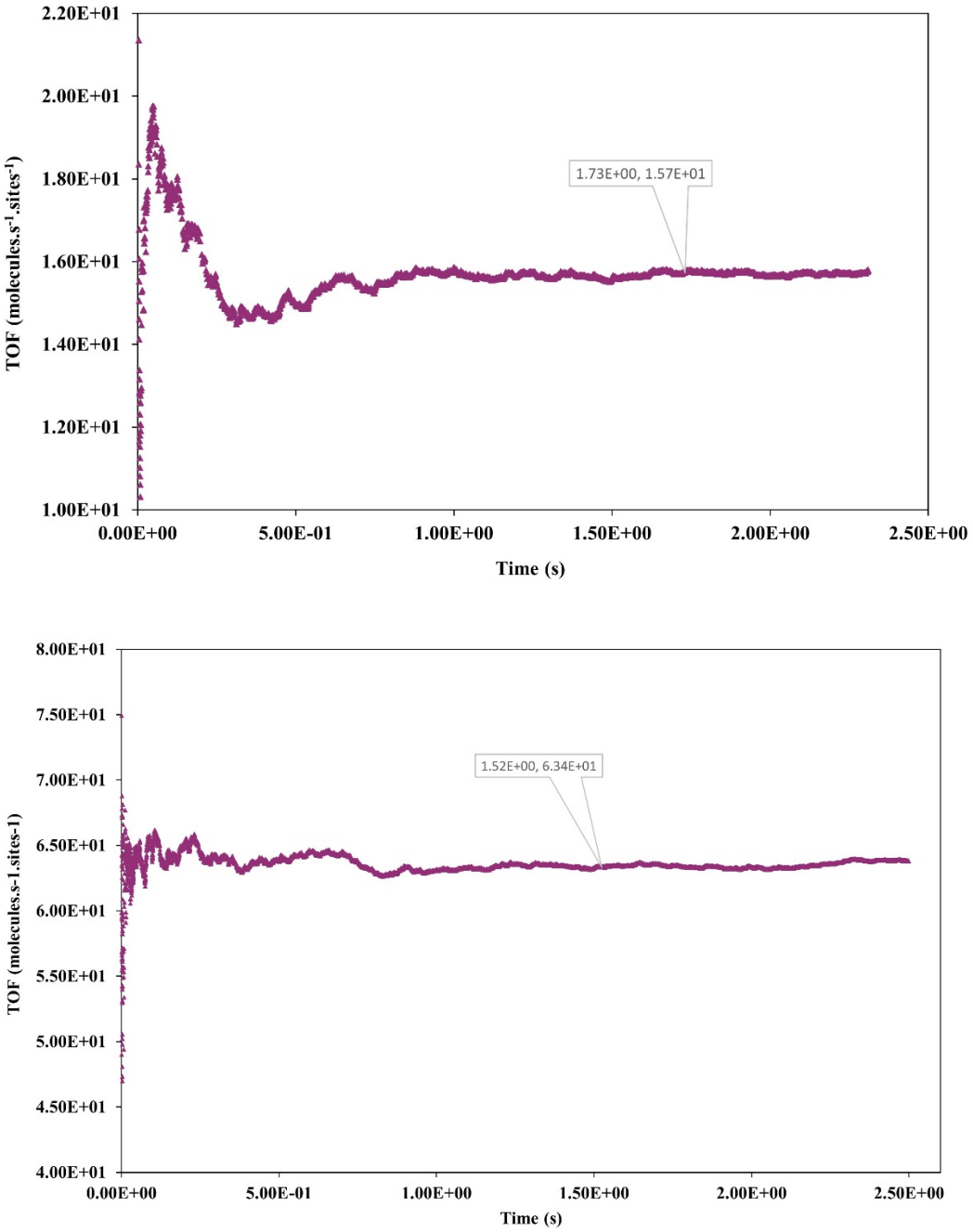


**Figure 5.** Convergence for the *k*MC simulations at 700 K (up) and 825 K (below).

**Supporting Table 1:** Elementary reactions in the *k*MC model and related parameters at 700 K and 1 bar of pressure with a $CO_2$:$CH_4$ mixture at a 1:1 ratio.

| Elementary reaction | $E_a$ (kJ·mol$^{-1}$) | $A_{forward}$ (s$^{-1}$) | $A_{reverse}$ (s$^{-1}$) | $k$ forward initial |
|---|---|---|---|---|
| $CO^*_{(hcp)} \leftrightarrow CO_{(g)} + *$ | 1.44 | 1.67E+15 | 1.93E+07 | 7.78E+04 |
| $CO^*_{(fcc)} \leftrightarrow CO_{(g)} + *$ | 1.40 | 1.33E+15 | 1.93E+07 | 1.20E+05 |
| $H^*_2 \leftrightarrow H_{2(g)} + *$ | 0.39 | 1.28E+13 | 7.21E+07 | 2.16E+10 |
| $H_2O^* \leftrightarrow H_2O_{(g)} + *$ | 0.27 | 1.06E+15 | 2.41E+07 | 1.23E+13 |
| $CO_{2(g)} + 2^* \leftrightarrow CO^*_{(hcp)} + O^*$ | **46.7** | 1.08E+05 | 1.21E+13 | 3.55E+01 |
| $CO_{2(g)} + 2^* \leftrightarrow CO^*_{(fcc)} + O^*$ | 46.7 | 1.08E+05 | 9.61E+12 | 3.55E+01 |
| $CH_{4(g)} + 2^* \leftrightarrow CH_3{}^* + H^*$ | **68.2** | 3.50E+07 | 3.14E+14 | 2.89E+02 |
| $CH_3{}^* + * \leftrightarrow CH_2{}^* + H^*$ | 26.6 | 1.67E+13 | 1.48E+13 | 1.72E+11 |
| $CH_2{}^* + * \leftrightarrow CH^* + H^*$ | 3.3 | 1.72E+13 | 1.45E+13 | 9.79E+12 |
| $CH^* + * \leftrightarrow C^* + H^*$ | 91.6 | 1.48E+13 | 1.72E+13 | 1.95E+10 |
| $C^* + O^* \leftrightarrow CO^* + *$ | **166.8** | 1.27E+13 | 1.95E+12 | 4.60E+00 |
| $CH^* + O^* \leftrightarrow HCO^* + *$ | **155.9** | 1.32E+13 | 3.05E+12 | 3.06E+01 |
| $HCO^* + * \leftrightarrow CO^* + H^*$ | 30.6 | 1.02E+14 | 7.91E+13 | 5.33E+11 |
| $H^* + H^* \leftrightarrow H^*_2 + *$ | 51.0 | 1.79E+14 | 2.64E+13 | 2.78E+10 |
| $CO^*_2 + H^* \leftrightarrow dCOOH^* + *$ | 84.4 | 2.18E+05 | 1.82E+13 | 1.09E-01 |
| $dCOOH^* + * \leftrightarrow CO^* + OH^*$ | 128.4 | 1.96E+12 | 7.75E+11 | 5.12E+02 |
| $H^* + O^* \leftrightarrow OH^* + *$ | 119.9 | 2.83E+13 | 8.37E+12 | 3.18E+04 |
| $OH^* + H^* \leftrightarrow H_2O^* + *$ | 77.8 | 4.19E+13 | 3.13E+13 | 6.60E+07 |
| $OH^* + OH^* \leftrightarrow H_2O^* + O^*$ | 44.2 | 9.46E+12 | 1.20E+13 | 4.74E+09 |

**Supporting Figure 4**: Energy profile of DRM on the Rh (111) surface *via* CH Oxidation and C Oxidation pathways compared to the respective Gibbs Energy profile including the thermodynamic corrections at 973.15 K, the typical experimental conditions. When the Gibbs corrections are included the $CO_2$ activation becomes the highest energy barrier, contrary to the energy profile based only on electronic energies, where the CHO and CO formation correspond to the highest energy barriers for the CH and C Oxidation paths, respectively.

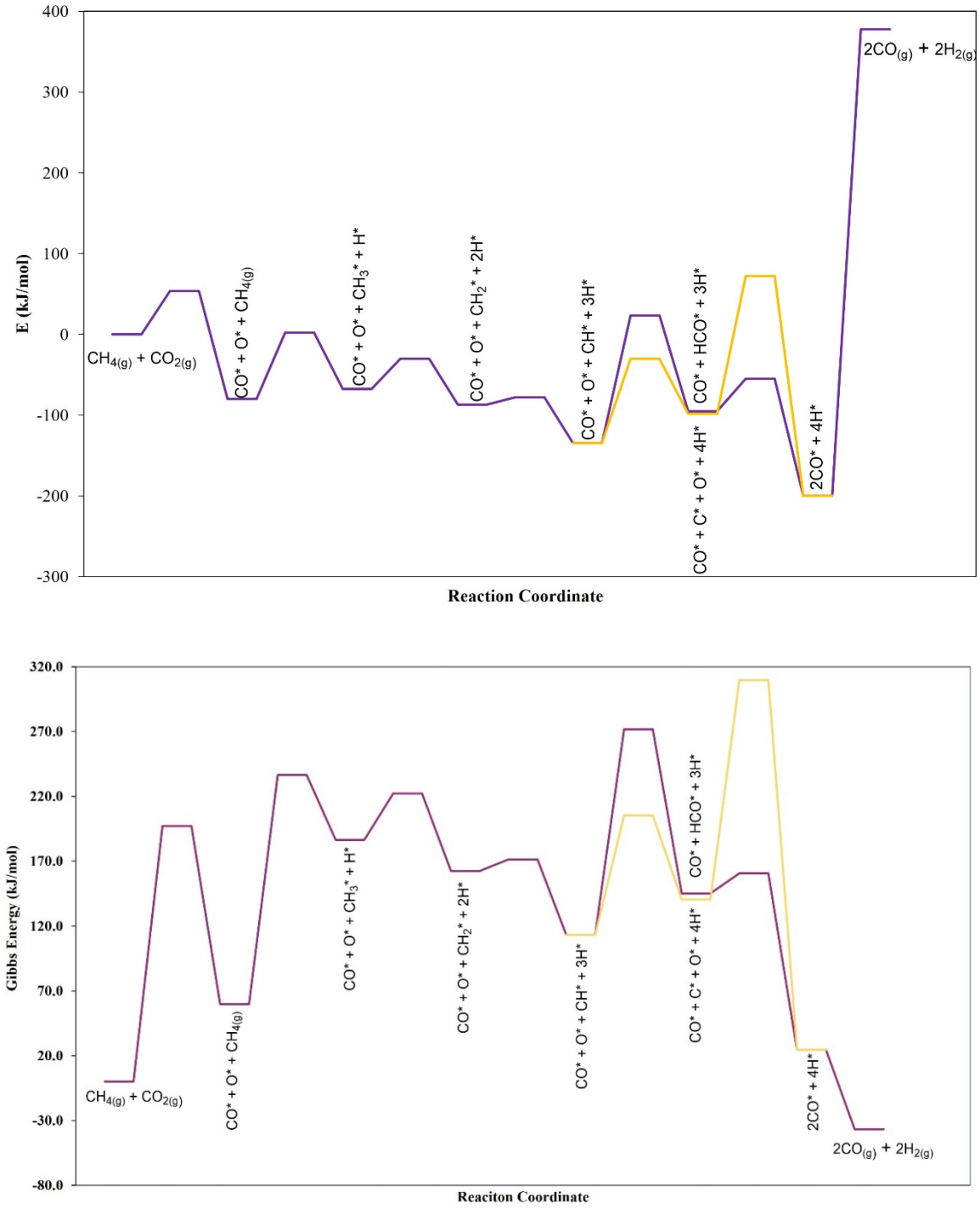


**Figure 4.** Energy profile of DRM on the Rh (111) surface via CH Oxidation (purple) and C Oxidation (yellow) path (up) and the respective Gibbs Energy profile (below) at 973 K.

**Supporting Figure 5**: Event frequency in the steady-state of the dry reforming of methane reaction at 973 K and 1 bar. The typical experimental conditions and the used ones to build the Gibbs energy

profile. At 973 K the system is more active with a TOF = 323 $s^{-1}$, as it is expected, but the trends are the same that those obtained in the range of temperatures studied in the main text.

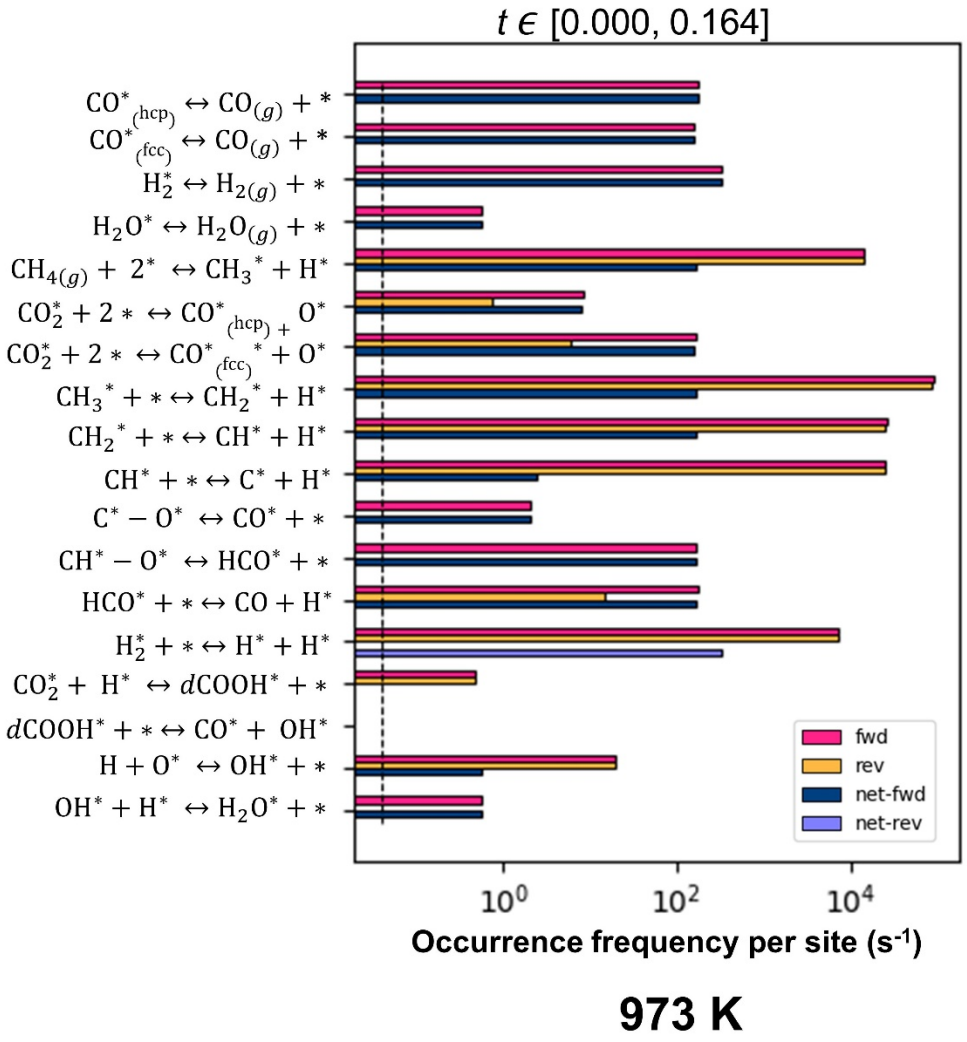


**Figure 5.** Event frequency of the dry reforming of methane reaction at 973 K and 1 bar.

**Supporting Figure 6**: TOF calculated as the slope of the number of CO molecules on the time per number of sites, after the steady-state is reached. This methodology was employed to find the TOF for all *k*MC simulations.

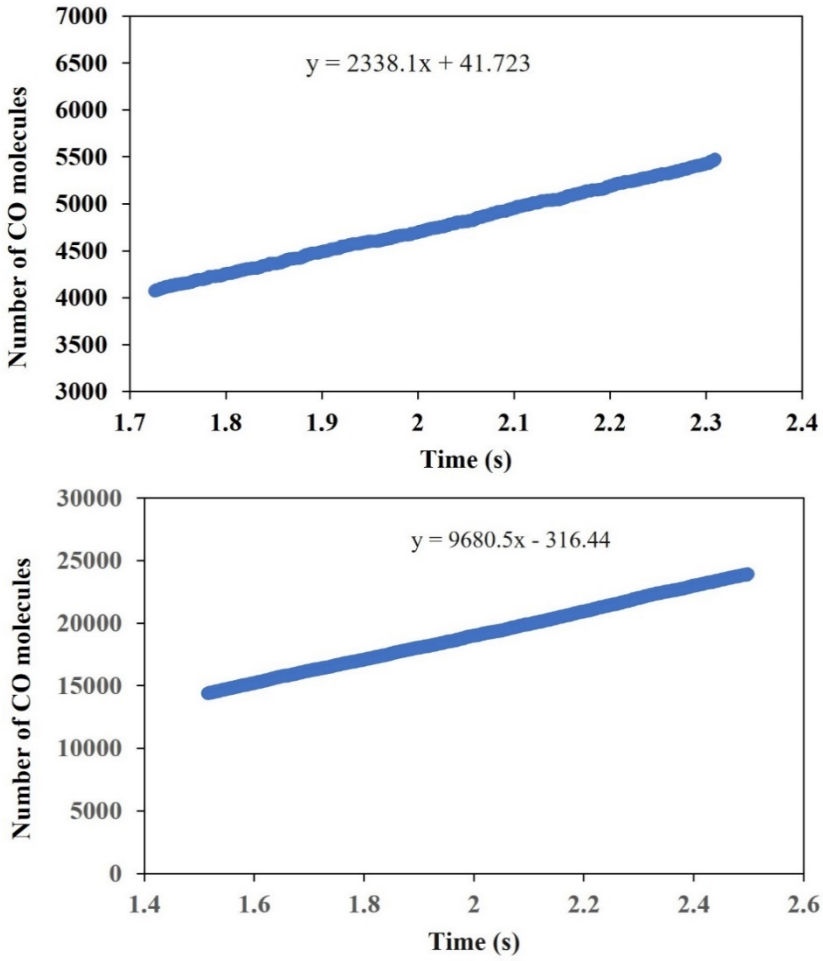


**Figure 6.** TOF calculated for the *k*MC simulations run at 700 K (up) and 825 K (below).

**Supporting Table 2:** TOF calculated, for all temperatures evaluated in this study, by means the previous method.

| Temperature | TOF calculated (molecules·sites$^{-1}$·s$^{-1}$) |
|---|---|
| 700 | 16 |
| 720 | 20 |
| 740 | 25 |
| 775 | 36 |
| 800 | 49 |
| 825 | 65 |

**Supporting Figure 7**: The polynomial method used to calculate the DRC for the $CO_2$ activation step, changing its energy barrier in a range from -0.15 eV to +0.10 for TOF of CO (up), $H_2$ (middle) and total (below). The DRC was calculated only at 700 K of temperature.

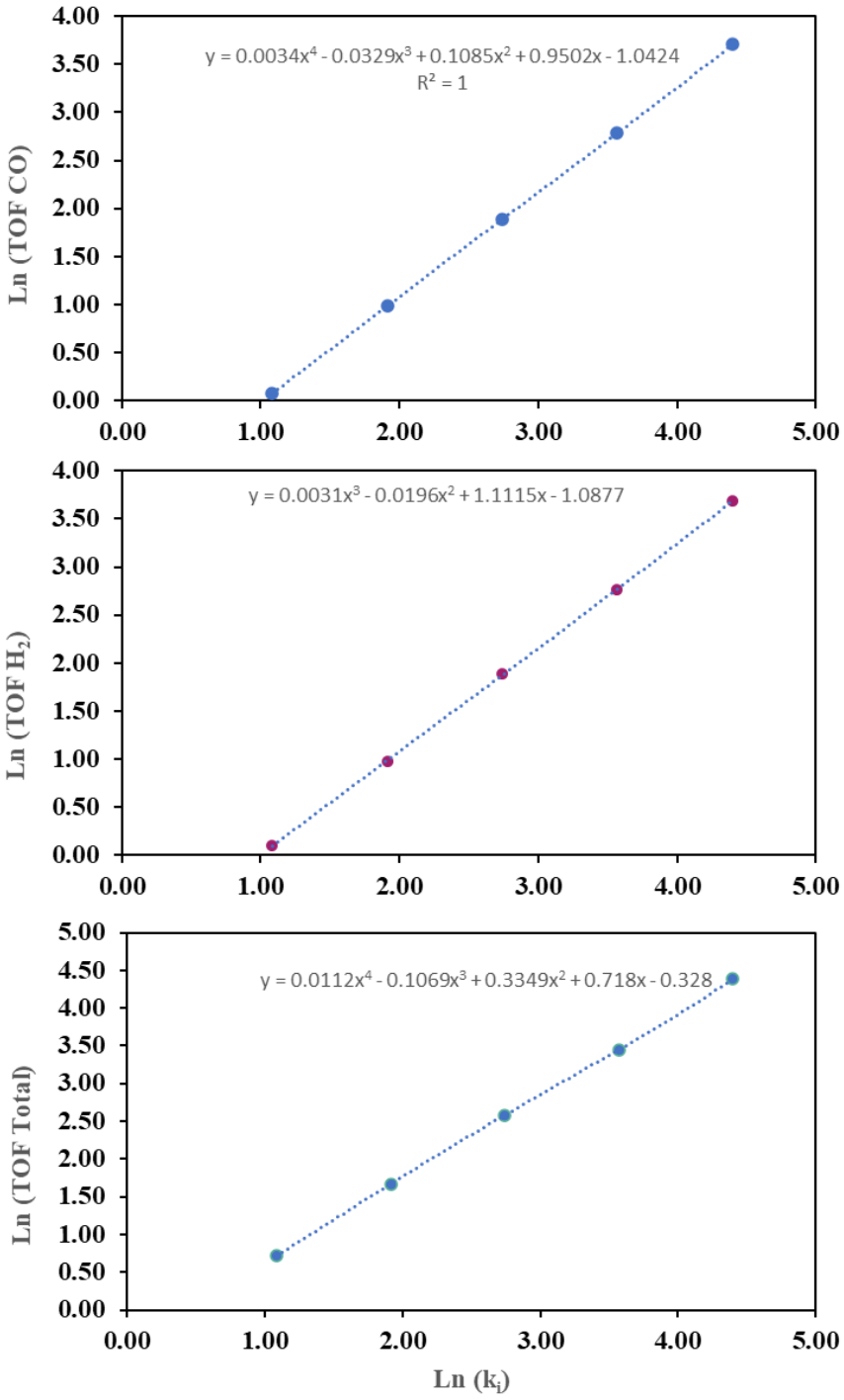


**Figure7.** DRC calculated for the $CO_2$ activation step run at 700 K for CO (up), $H_2$ (middle) and total (below) TOF.

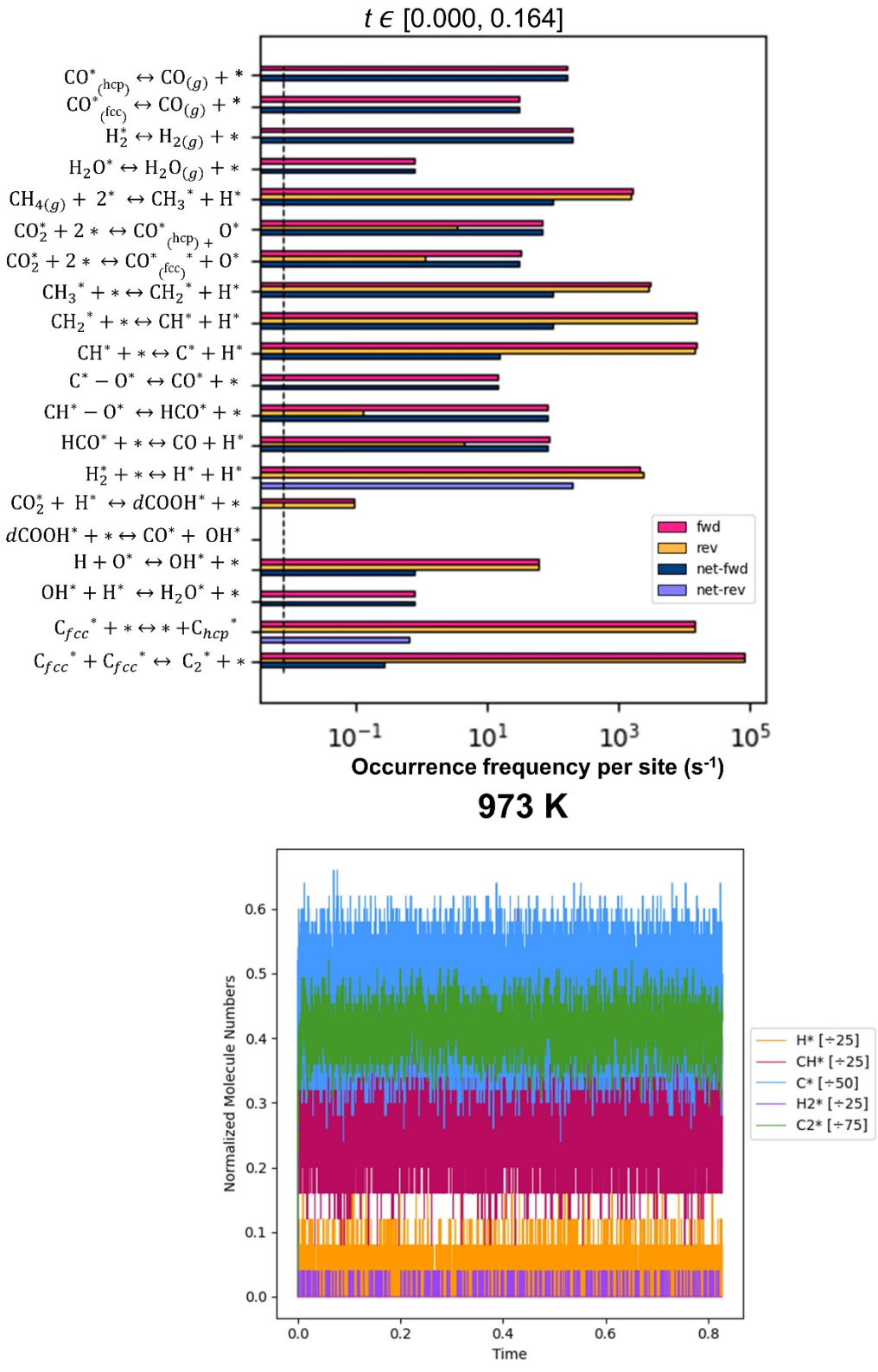


**Figure 8.** Event frequency per site (up) and surface coverage (below) of the DRM reaction at 973 K and 1 bar, including the C* migration and $C_2$* formation elementary reactions.

**Supporting Figure 8**: Event frequency per site in the steady-state of the dry reforming of methane reaction at 973 K and 1 bar. Before including the elementary reactions mentioned in the following table, the system is more active with a TOF = 323 $s^{-1}$. After including the reactions, the *k*MC simulation shows (as shown figure below) that the $C_2$* formation is occurring but with a lower net-forward occurrence frequency than that to produce CO* via C/CH* oxidation paths. Therefore, the system remains active to produce DRM products but at smaller TOF (194 $s^{-1}$) due to the inclusion of another reaction consuming C*. Furthermore, the $C_2$* was found to have a significant coverage on the surface but without evidence of catalyst deactivation.

| Elementary step | $\Delta E^{\neq}$ (kJ·mol$^{-1}$) | $A_{forward}$ |
|---|---|---|
| $C_{hcp}$* + * ↔ * + $C_{fcc}$* | 61 | 8.5E+12 |
| $C_{fcc}$* + $C_{fcc}$ * ↔ $C_2$* + * | 133 | 1.6E+13 |

**Supporting Figure 9**: Event frequency per site in the steady-state of the dry reforming of methane reaction at 973 K and 1 bar. We considered the inclusion of a reaction to produce $CH_2O$* as a key intermediate, which can also lead to the formation of the main DRM products, CO and $H_2$. However, the inclusion of this new elementary reaction (shown in the table below) did not alter the results observed. The following table shows the barrier energy (including ZPE correction) to produce $CH_2O$*, is comparable to that for CO formation, as can be seen in the supporting Table 1. However, the $k_{forward}$ is higher for CO formation (1.67E+04) than that for $CH_2O$* formation (1.08E+04) at 973 K.

| Elementary step | $\Delta E^{\neq}$ (kJ·mol$^{-1}$) | $A_{forward}$ |
|---|---|---|
| $CH_2$* + O* ↔ $CH_2O$* + * | 166 | 9.1E+12 |

The **supporting Figure 9** shows the *k*MC simulation carried out at 973 K of the system after including $CH_2O$ formation. According to the results, we can conclude that the system keeps the same catalytic activity as the $CH_2O$* formation is not occurring and does not affect kinetics. In the same way, the

coverage of the species is practically the same, with barely appreciable differences that do not lead to relevant changes.

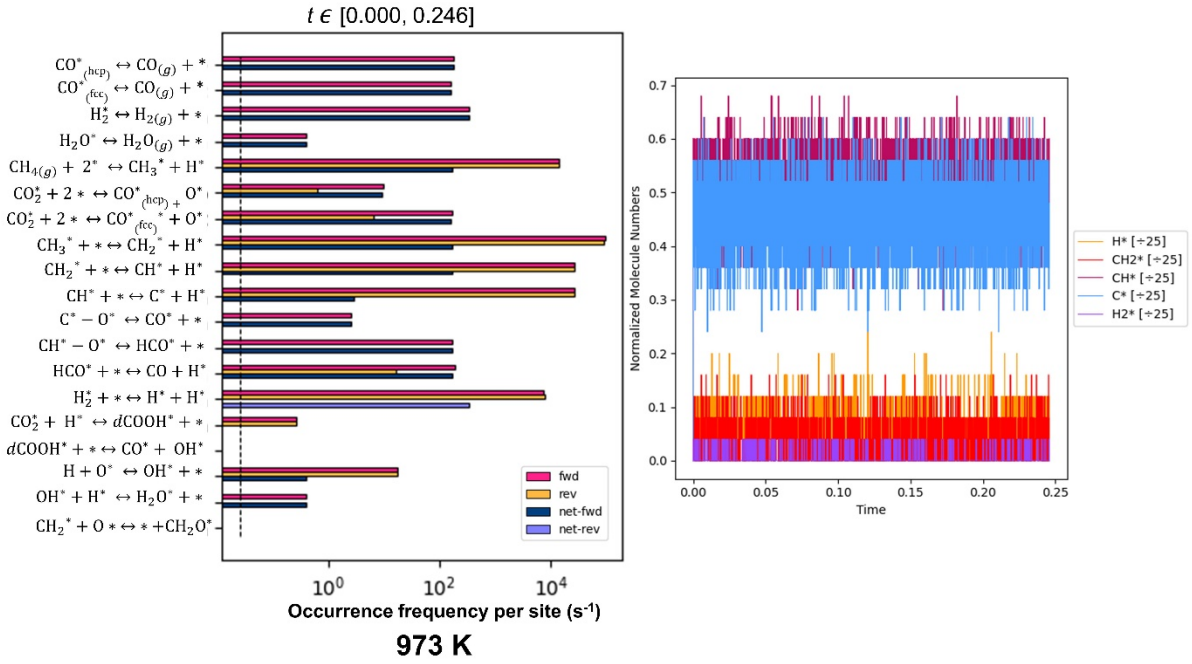


**Figure 9.** Event frequency per site (left) and surface coverage (right) of the DRM reaction at 973 K and 1 bar, including the $CH_2O*$ formation elementary reaction.

## References:


1 J. C. Woolley, *Introduction to solid state physics*, 1957, vol. 6.

2 D. A. McQuarrie, *Statistical mechanics / Donald A. McQuarrie*, 1975.

3 J. Nielsen, M. D'Avezac, J. Hetherington and M. Stamatakis, *J. Chem. Phys.*, 2013, **139**, 1–13.